Observation of $^1S_0$-$^3P_0$ transition of bosonic strontium in the Lamb-Dicke regime

Qinfang Xu (徐琴芳)[1], Hui Liu (刘 辉)[1,2], Benquan Lu (卢本全)[1,2], Yebing Wang (王叶兵)[1], Mojuan Yin (尹默娟)[1], Dehuan Kong (孔德欢)[1], Jie Ren (任 洁)[1], Xiao Tian (田 晓)[1], and Hong Chang (常 宏)[1,*]

[1]*CAS Key Laboratory of Time and Frequency Primary Standards, National Time Service Center, Xi'an 710600, China*
[2]*University of Chinese Academy of Sciences, Beijing 100049, China*
**Corresponding author: changhong@ntsc.ac.cn*

Received May 7, 2015; accepted July 31, 2015; posted online August 31, 2015

We report experiments on the observation of the $^1S_0 - {}^3P_0$ transition spectrum of ^{88}Sr in the Lamb-Dicke regime. After going through a two-stage magneto-optical trap (MOT), ^{88}Sr cold atoms with number of about 1×10^5 and a longitudinal temperature of 8.4 μK are loaded into a one-dimensional (1D) optical lattice, which is realized with a semiconductor laser at 813.4 nm. Using the magnetic field-inducing $^3P_1$ state mixing into $^3P_0$ state, the spectroscopy of the $^1S_0 - {}^3P_0$ transition with a linewidth of 180 Hz is detected.

OCIS codes: 020.7010, 140.3320, 020.1335, 020.3320.
doi: 10.3788/COL201513.100201.

The appearance of the atom optical lattice clock has strongly promoted developments in the area of optical frequency standards[1–4]. Due to the high performance in its stability and accuracy, the optical frequency standards may improve the level of measurement of basic physical constants[5], such as the measurement of the fine-structure constant and temporal drifts[6]. Furthermore, the improved timing standards open up some new applications, including chronometric leveling-based geodesy[7], navigation[8], and space travel[9]. So far, there are lots of institutes researching the optical lattice clock with different species of atoms, such as strontium (Sr)[10–15] and ytterbium (Yb)[16–20]. Optical lattice clocks with many ultra-cold atoms confined in optical lattices operating on the magic wavelength[21] have great precision. To date, the best optical lattice clocks have been achieved to a 10^{-18} level with total uncertainty[22,23]. Among these optical lattice clocks, fermionic ^{87}Sr has an ultra-narrow transition when realizing high-precision optical lattice clocks[24–27]. On account of the natural abundance and the simplicity of the energy structure of bosonic ^{88}Sr, some institutes also selected it to make the optical lattice clock, which has resulted in a much easier cooling process and higher cooling efficiency[28,29].

In this Letter, we demonstrate our experiments on the observation of the $^1S_0 - {}^3P_0$ transition of ^{88}Sr in the Lamb-Dicke regime. We have prepared cold atomic samples, confined atoms in the Lamb-Dicke regime with the magic wavelength, and probed the $^1S_0 - {}^3P_0$ transition spectrum with a normalized detection method.

The energy level scheme of strontium is shown in Fig. 1. The strontium atoms are cooled in a two-stage magneto-optical trap (MOT). The first stage MOT is based on the strong transition of $^1S_0 - {}^1P_1$, whose emission wavelength is at 461 nm, and whose Doppler cooling limit temperature is 108 μK. To prevent the loss of atoms via $^1P_1 - {}^1D_2 - {}^3P_2$, two lasers at 679 and 707 nm are employed to repump the atoms to the $^3P_1$ state. Then, the atoms decay to the $^1S_0$ state. The second stage MOT is based on the inter-combination transition of $^1S_0 - {}^3P_1$, which has an emission wavelength of 689 nm and has a natural linewidth of merely 7.6 kHz, corresponding to a Doppler cooling limit temperature of 180 nK. For bosonic strontium, the $^1S_0 - {}^3P_0$ transition is rigorously forbidden[30]. A static magnetic field can be used to induce the $^3P_1$ state into the $^3P_0$ state and make the $^1S_0 - {}^3P_0$ transition possible in ^{88}Sr[31].

The experimental setup is shown in Fig. 2. The system for the first stage MOT had been reported in detail in Ref. [32]. The number of atoms in the first stage MOT is achieved to the 10^8 level, and the temperature is about 3 mK. Exploring $^1S_0 - {}^3P_1$ narrow line dynamics at 689 nm requires a laser system whose linewidth needs to be narrow compared to the 7.6 kHz natural transition linewidth. In our experiment, the 689 nm laser is narrowed by locking it to a stable, optical reference, ultra-low expansion (ULE) cavity (Finesse 12000) via the Pound–Drever–Hall (PDH) technique. The linewidth of the 689 nm laser is

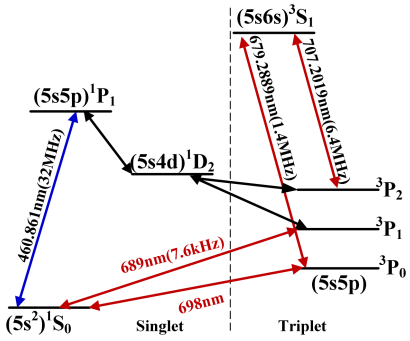

Fig. 1. Energy level scheme of the ^{88}Sr atom.

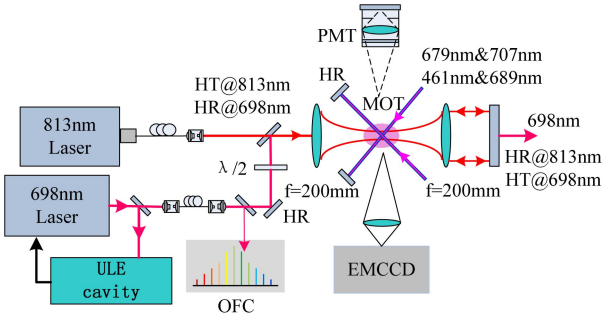

Fig. 2. Experimental setup. PMT: photomultiplier tube. EMCCD: electron multiplying charge-coupled device. OFC: optical frequency comb.

narrowed to about 200 Hz[33]. A one-dimensional (1D) optical lattice is realized with an 813 nm laser, which is a diode laser with tapered amplifier (TA) laser system. After passing through a single-mode polarization-maintaining fiber, the maximum output power of the 813 nm laser is 950 mW. The lattice laser is tightly focused by an achromatic lens that has a focal length of 200 mm, and the beam waist is about 38 μm. Then, the incident beam is retro-reflected by the same lens and a reflector. In order to make the returning beam overlap and maintain the same beam parameters as the original incident beam, the fiber splitter is used to make sure the incident beam strictly overlaps the retro-reflected beam. Then, a horizontally oriented 1D optical lattice is realized with the 813 nm diode laser. A 698 nm commercial laser is used as the clock laser. The frequency of the 698 nm laser is locked to a ULE cavity (Finesse 400,000) via the PDH technique. The linewidth of the clock laser system is 0.5 Hz, and the fractional Allan deviation is 1×10^{-15} at 1 s.

The experiment for the 698 nm clock transition is controlled by the time sequence shown in Fig. 3. After the first stage MOT, the magnetic field gradient is rapidly reduced from 50 to 3 G/cm. At a 50 kHz modulation frequency and

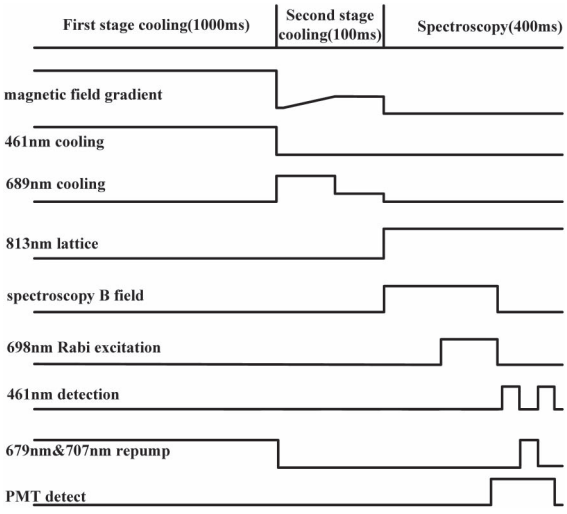

Fig. 3. Time sequence of the experiment for the 698 nm clock transition.

a 1.8 MHz frequency deviation, the 689 nm laser is modulated into a broadband width to match the thermal distribution of the atoms, which have been prepared in the first stage MOT. Meanwhile, the magnetic field is ramped up to 10 G/cm in 50 ms to compress the volume of the atomic cloud. After the frequency modulation has been switched off, within 50 ms of single-frequency laser cooling, the loading efficiency into the second stage MOT is about 15%. Approximately 10^7 atoms are trapped at about 2 μK. At the end of the second stage MOT, the magnetic field is switched off.

After two-stage MOT, we switched on the 813 nm laser, and strontium atoms are loaded into the optical lattice when their temperature is reduced to be lower than the trap depth of the lattice. The magic wavelength of the strontium optical lattice makes the first-order AC Stark shifts of the ground and the excited states equal. Theoretically, with the 813 nm beam waist of 38 μm and a power of 850 mW, a trap depth of 95 μK can be realized, and the longitudinal and transverse trap frequencies are 166 kHz and 800 Hz, respectively.

Figure 4 is the picture of the atoms loaded into the 1D optical lattice within 30 ms, which is recorded by an electron-multiplying charge-coupled device (EMCCD, Andor DU-897) with the 461 nm probe beam. Part of the atoms, whose temperature is lower than the trap depth of the lattice, are trapped in the optical lattice due to the dipole potential, while the rest of the atoms fall down due to gravity. The size of the picture recorded by the EMCCD is 5.12 mm × 5.12 mm, the resolution ratio is 320 × 320, the pixel size is 0.016 mm, and the magnification is 1. According to the atomic fluorescence intensity distribution in the picture, we estimate the half width of the atoms in the optical lattice to be about 40 μm, which is close to 813 nm beam waist of 38 μm. This means that part of the cold atoms are loaded into the near region of the beam waist. Based on the number of atoms in the second stage MOT, by comparing the atomic fluorescence intensity distribution before and after loading, the number of atoms can be estimated to be about 1×10^5.

Also, we use a photomultiplier tube to measure the fluorescence intensity of the atomic cloud in the optical lattice and evaluate the lifetime of the atoms. In order to eliminate the stray light and obtain a high signal-to-noise ratio

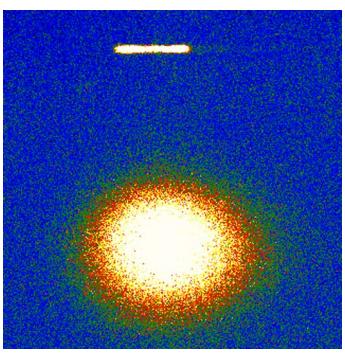

Fig. 4. Picture of the optical lattice-loaded atoms.

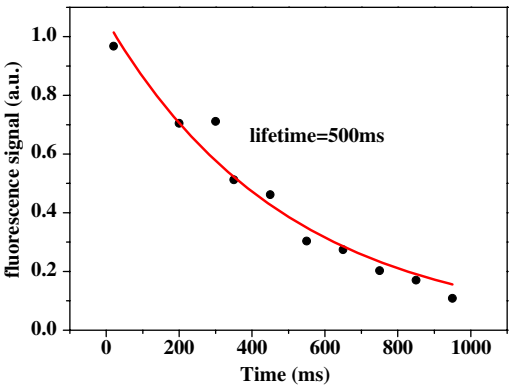

Fig. 5. Lifetime of the atoms in the 1D optical lattice.

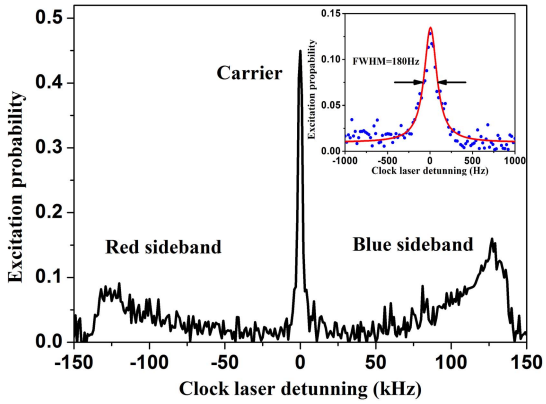

Fig. 6. Clock transition spectrum. The black curve with the resolved sideband is the clock transition's wide spectrum swept by a 1 kHz step size. The inset shows the narrow spectrum of the transition with a FWHM of 180 Hz; the solid red curve is a Lorentzian fit to the data yields.

(SNR) for the fluorescence intensity, a 461 nm filter, a lens group, and an aperture are used to eliminate the background noise. In this way, we measure the fluorescence intensity of the atomic cloud in the optical lattice, as shown in Fig. 5. The black points represent the fluorescence intensity of the atomic cloud in the optical lattice at different probe times. The red solid curve is an exponential function fit to the data yields. The lifetime of the atoms trapped in the 1D optical lattice is 500 ms.

Utilizing the ultra-narrow feature of the $^1S_0 - {}^3P_0$ as the clock transition, and considering that an ^{88}Sr clock transition $^1S_0 - {}^3P_0$ is rigorously forbidden, we apply a static magnetic field to mix a small and controllable fraction of the nearby $^3P_1$ state into the $^3P_0$ state to quench the forbidden transition, with a Rabi frequency[34], as follows:

$$\Omega_R = \alpha\sqrt{I}|B|, \tag{1}$$

where $\alpha(\mathrm{Sr}) = 198\ \mathrm{Hz}/(\mathrm{T}\sqrt{\mathrm{mW}\cdot\mathrm{cm}^{-2}})$, B is the magnetic field intensity, and I is the intensity of the probe light at 698 nm.

The frequency of the 698 nm laser was accurately measured by an optical frequency comb (OFC, Menlo FC1500). Moreover, an acoustic optical modulator was employed to shift the frequency of the 698 nm laser to a reference frequency[35]. As shown in Fig. 3, after the two stages of cooling, the anti-Helmholtz coils are changed into a Helmholtz configuration by reversing one of the coils' currents. The 698 nm clock laser is switched on to induce the clock transition. In order to increase the SNR of the Rabi excitation measurement, a normalized detection method is applied. The first resonant 461 nm imaging beam pulse (4 ms) is switched on to detect the atoms remaining in the $^1S_0$ state after the clock transition interrogation. The measured $^1S_0$ atomic population is n_1. At the same time, the atoms in $^1S_0$ are wiped out of the optical lattice after the first 461 nm pulse. The atoms excited into the $^3P_0$ state by the clock laser beam are pumped back into the $^1S_0$ state within 4 ms by pulses at 707 and 679 nm. After the second 461 nm pulse (4 ms), the $^3P_0$ atomic population is measured to be n_2. Finally, the excitation probability is given by the ratio $r = n_2/(n_1 + n_2)$.

The wide-scan spectrum obtained is shown in Fig. 6. It was achieved by using a static magnetic field of $B = 24$ mT and a 698 nm clock laser intensity of 16 W/cm^2. The Rabi frequency is estimated to be about 600 Hz. We set the clock laser frequency to change with scan steps of 1 kHz, and the pulse length of clock laser at 698 nm is 90 ms. The clock transition spectrum is composed of the carrier and sideband transition, which are shown as the black curve. The sideband transitions correspond to the transitions to the +1 and −1 motional states (the blue and red sidebands). The full width at half-maximum (FWHM) of the carrier transition is about 3 kHz from the wide spectrum. The motional sideband spectrum exhibits some features similar to the harmonically trapped atoms. The trap frequency along the longitudinal axis (ν_z, measured approximately from the peak of the sideband to the carrier transition) is about 130 kHz. Thus, our experiment corresponds to the Lamb-Dicke parameters[34] of $\eta = \sqrt{\nu_R/\nu_z} \approx 0.19$, where $\nu_R = h/(2M\lambda^2)$ is the atomic recoil frequency shift associated with the absorption of a photon and $\lambda = 698$ nm. The trap depth is 67 μK. This takes into account that the beam waist and the center of the second stage MOT do not strictly overlap. The experimental value of 67 μK is less than the theoretical value of 95 μK. Moreover, the amplitudes of the blue and red sidebands in the transition spectrum are weighted by the population distribution. The atomic sample temperature is given by the equation[36]

$$\frac{P_{\mathrm{red}}}{P_{\mathrm{blue}}} \approx \frac{N_1}{N_0} = e^{-\frac{\hbar\nu_z}{\kappa_B T}}, \tag{2}$$

where P_{red} and P_{blue} are the peak amplitudes of the red and blue sidebands, and N_0 and N_1 are the atomic populations in the ground and first excited $^1S_0$ motional

states. We calculated the longitudinal temperature of the trapped atoms to be about 8.4 μK.

The narrow spectrum can be obtained by reducing the laser intensity and the magnetic field B. Considering the SNR, we kept the same pulse length of the clock laser at 698 nm with 90 ms. We also set the clock laser intensity and the magnetic field B to about 5 W/cm^2 and 0.8 mT, respectively. The inset in Fig. 6 is the narrow spectrum observed under this experimental condition. The blue points denote the values of the clock transition measurement, and the red solid curve represents a Lorentzian fit to the data yields. The linewidth of the narrow transition spectrum is 180 Hz. In our experiment, the spectroscopic linewidth is limited by the power broadening due to the clock laser, lattice decoherence effects, and the effective Rabi frequency.

With a static magnetic field of $B = 24$ mT and the clock laser at 698 nm with an intensity of 3.6 W/cm^2, by changing the clock laser pulse length, the Rabi oscillations are obtained. By fitting the Rabi oscillations, we get the Rabi spectroscopy of the clock transition shown in Fig. 7. The black points denote the values of the Rabi excitation measurement with different clock pulse lengths. The red solid curve is the result by fitting with the function $a(1-\cos(2\pi\Omega_{\mathrm{FIT}}\Delta t)\exp(\Delta t/\tau_{\mathrm{FIT}}))$. On the carrier, the Rabi π-pulse excitation at 5 ms shows a nearly 65% excitation of atoms, the measured atomic Rabi frequency Ω_{FIT} is 165 Hz, which is about 58% of the estimated Rabi frequency Ω_R calculated from the magnetic field and the clock laser intensity (see Eq. 1). These results are owing to the inhomogeneous excitation among the atoms by some experimental factors[37], such as the residual misalignment between the lattice beam and the 698 nm clock beam axes, the 698 nm clock beam induced residual spatial inhomogeneities and the transverse motion dependence on the atomic temperature in the optical lattice. We can find the decoherent time τ_{FIT}, which is relevant to the thermal atomic collisions[36], is 5 ms with the fitting curve.

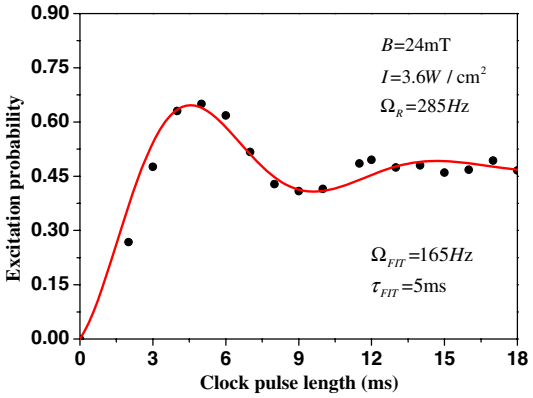

Fig. 7. Measurement of the Rabi oscillation. The data are fitted with the function $a(1-\cos(2\pi\Omega_{\mathrm{FIT}}\Delta t)\exp(\Delta t/\tau_{\mathrm{FIT}}))$ from Ref. [37], where Ω_{FIT} is the actual atomic Rabi frequency and τ_{FIT} gives the decoherent time scale.

In conclusion, we load strontium atoms into a 1D optical lattice, and then use magnetic field-induced spectroscopy on ^{88}Sr to obtain the clock transition spectrum with sideband. By reducing the magnetic field B and the intensity of the probe laser, the spectrum of the transition at 180 Hz in the experiment is obtained. Upon observing the Rabi oscillations, due to inhomogeneous excitation among the atoms, we see that the Rabi π-pulse excitation at 5 ms shows a nearly 65% excitation of atoms.

This work was supported by the National Nature Science Foundation of China (Nos. 61127901 and 11474282) and the Key Project of the Chinese Academy of Sciences (No. KJZD-EW-W02).

References

1. H. Katori, in *Proceedings of the 6th Symposium on Frequency Standards and Metrology* 323 (2002).
2. M. Takamoto, F. L. Hong, R. Higashi, and H. Katori, Nature **435**, 321 (2005).
3. W. Xiong, Y. Zhang, Z. Ma, and X. Chen, Chin. Opt. Lett. **10**, 090201 (2012).
4. J. Wan, H. Cheng, Y. Meng, L. Xiao, P. Liu, X. Wang, Y. Wang, and L. Liu, Chin. Opt. Lett. **13**, 020201 (2015).
5. C. J. Bordé, Phil. Trans. R. Soc. A **363**, 2177 (2005).
6. S. Blatt, A. D. Ludlow, G. K. Campbell, J. W. Thomsen, T. Zelevinsky, M. M. Boyd, J. Ye, X. Baillard, M. Fouché, R. Le Targat, A. Brusch, P. Lemonde, M. Takamoto, F. L. Hong, H. Katori, and V. V. Flambaum, Phys. Rev. Lett. **100**, 140801 (2008).
7. C. W. Chou, D. B. Hume, T. Rosenband, and D. J. Wineland, Science **329**, 1630 (2010).
8. T. M. Fortier, M. S. Kirchner, F. Quinlan, J. Taylor, J. C. Bergquist, T. Rosenband, N. Lemke, A. Ludlow, Y. Jiang, C. W. Oates, and S. A. Diddams, Nat. Photon. **5**, 425 (2011).
9. D. Kleppner, Phys. Today **59**, 10 (2006).
10. R. L. Targat, X. Baillard, M. Fouché, A. Brusch, O. Tcherbakoff, G. D. Rovera, and P. Lemonde, Phys. Rev. Lett. **97**, 130801 (2006).
11. M. Takamoto, F. L. Hong, R. Higashi, Y. Fujii, M. Imae, and H. Katori, J. Phys. Soc. Jpn. **75**, 104302 (2006).
12. M. M. Boyd, A. D. Ludlow, S. M. Foreman, S. Blatt, T. Ido, T. Zelevinsky, and J. Ye, Phys. Rev. Lett. **98**, 083002 (2007).
13. N. Poli, C. W. Oates, P. Gill, and G. M. Tino, Rivista del Nuovo Cimento **36**, 555 (2013).
14. B. J. Bloom, T. L. Nicholson, J. R. Williams, S. L. Campbell, M. Bishof, X. Zhang, W. Zhang, S. L. Bromley, and J. Ye, Nature **506**, 71 (2014).
15. Y. G. Lin, Q. Wang, Y. Li, B. K. Lin, S. K. Wang, F. Meng, Y. Zhao, J. P. Cao, E. J. Zang, T. C. Li, and Z. J. Fang, Chin. Phys. Lett. **30**, 014206 (2013).
16. M. Zhou, N. Chen, X. H. Zhang, L. Y. Huang, M. F. Yao, J. Tian, Q. Gao, H. L. Jiang, H. Y. Tang, and X. Y. Xu, Chin. Phys. B **22**, 103701 (2013).
17. S. G. Porsev, A. Derevianko, and E. N. Fortson, Phys. Rev. A **69**, 021403(R) (2004).
18. C. W. Hoyt, Z. W. Barber, C. W. Oates, T. M. Fortier, S. A. Diddams, and L. Hollberg, Phys. Rev. Lett. **95**, 083003 (2005).
19. T. Hong, C. Cramer, E. Cook, W. Nagourney, and E. N. Fortson, Opt. Lett. **30**, 2644 (2005).
20. N. Poli, Z. W. Barber, N. D. Lemke, C. W. Oates, L. S. Ma, J. E. Stalnaker, T. M. Fortier, S. A. Diddams, L. Hollberg, J. C. Bergquist, A. Brusch, S. Jefferts, I. Heavner, and I. Parker, Phys. Rev. A **77**, 050501(R) (2008).

21. T. Ido and H. Katori, Phys. Rev. Lett. **91**, 053001 (2003).
22. T. L. Nicholson, S. L. Campbell, R. B. Hutson, G. E. Marti, B. J. Bloom, R. L. McNally, W. Zhang, M. D. Barrett, M. S. Safronova, G. F. Strouse, W. L. Tew, and J. Ye, Nat. Commun. **6**, 6896 (2015).
23. B. J. Bloom, T. L. Nicholson, J. R. Williams, S. L. Campbell, M. Bishof, X. Zhang, W. Zhang, S. L. Bromley, and J. Ye, Nature **506**, 71 (2014).
24. T. Akatsuka, M. Takamoto, and H. Katori, Nat. Phys. **4**, 954 (2008).
25. G. K. Campbell, A. D. Ludlow, and S. Blatt, Metrologia **45**, 539 (2008).
26. X. Baillard, M. Fouché, R. L. Targat, P. G. Westergaard, A. Lecallier, F. Chapelet, M. Abgrall, G. D. Rovera, P. Laurent, P. Rosenbusch, S. Bize, G. Santarelli, A. Clairon, P. Lemonde, G. Grosche, B. Lipphardt, and H. Schnatz, Eur. Phys. J. D. **48**, 11 (2008).
27. S. Falke, H. Schnatz, J. S. R. Vellore Winfred, T. Middelmann, S. Vogt, S. Weyers, B. Lipphardt, G. Grosche, F. Riehle, U. Sterr, and C. Lisdat, Metrologia **48**, 399 (2011).
28. T. Akatsuka, M. Takamoto, and H. Katori, Phys. Rev. A **81**, 023402 (2010).
29. M. G. Tarallo, N. Poli, M. Schioppo, D. Sutyrin, and G. M. Tino, Appl. Phys. B **103**, 17 (2011).
30. X. Baillard, M. Fouché, R. L. Targat, P. G. Westergaard, A. Lecallier, Y. L. Coq, G. D. Rovera, S. Bize, and P. Lemonde, Opt. Lett. **32**, 1812 (2007).
31. V. Taichenachev, V. I. Yudin, C. W. Oates, C. W. Hoyt, Z. W. Barber, and L. Hollberg, Phys. Rev. Lett. **96**, 083001 (2006).
32. H. Chang, S. G. Zhang, X. L. Wang, and X. Tian, Scientia Sinica Phys. Mech & Astron. **40**, 616 (2010).
33. F. Gao, H. Liu, P. Xu, X. Tian, Y. Wang, J. Ren, H. B. Wu, and H. Chang, AIP Adv. **4**, 027118 (2014).
34. N. Poli, M. Schioppo, S. Vogt, S. Falke, U. Sterr, C. Lisdat, and G. M. Tino, Appl. Phys. B **117**, 1107 (2014).
35. X. Baillard, M. Fouché, R. L. Targat, P. G. Westergaard, A. Lecallier, Y. L. Coq, G. D. Rovera, S. Bize, and P. Lemonde, Opt. Lett. **32**, 1812 (2007).
36. D. Ludlow, "The Strontium Optical Lattice Clock: Optical Spectroscopy with Sub-Hertz Accuracy," Ph.D. thesis, University of Colorado (2008).
37. S. Blatt, J. W. Thomsen, G. K. Campbell, A. D. Ludlow, M. D. Swallows, M. J. Martin, M. M. Boyd, and J. Ye, Phys. Rev. A. **80**, 052703 (2009).